Dense simple plasmas as high-temperature liquid simple metals

F. Perrot
Centre d'Etudes de Limeil-Valenton, 94195 Villeneuve-St. Georges CEDEX, France
and Institute for Theoretical Physics, University of California, Santa Barbara, California 93106
(Received 8 November 1989)

In this paper, we study the thermodynamic properties of dense plasmas considered as high-temperature liquid metals. The problems that have to be solved are the following: (1) calculation of the "average" electron-density profile around an ion in the plasma, (2) determination of a self-consistent average ionization of the plasma, (3) calculation of the pair interaction between two ions, and (4) calculation of the total Helmholtz free energy. The first point is approximately solved in the Mermin-Kohn-Sham (MKS) density-functional theory of thermal ensembles, for a single ion in a spherical cavity in jellium. A prescription is then proposed for calculating the average ionization as a function of density and temperature using the electron densities from the MKS scheme. This prescription is shown to work well when the electron structure of the plasma is simple (i.e., when the overlap of bound states is not too large, and when there is no resonance in the free spectrum). The use of a superposition of single-ion densities for the total charge density of the plasma, together with a cluster expansion of the kinetic and exchange-plus-correlation energy, leads to the definition of the pair interaction that is readily calculable. Finally, the structural (ionic) part of the free energy is obtained from the hypernetted-chain theory of fluids.

I. INTRODUCTION

Studies of the thermodynamics of plasmas are currently based almost always on the notion of pair interactions $\phi(R)$ and pair-correlation functions $g(R)$. Extensive calculations of the thermodynamic functions have been made in the past, using simple model potentials, such as bare[1-3] or screened Coulomb interactions.[4-7] Self-consistent pair potentials have also been carefully determined in the case of light, fully ionized materials,[8,9] covering quite a wide range of densities and temperatures. It seems now of some importance to relate these approaches to a number of models currently used in conventional condensed-matter physics, where much work has been done on ion-ion interactions in metals, with application to structures of liquid metals, alloys, impurities and vacancies, phonon spectra, etc.[10] The aim of this paper is to show that, in some cases, the solid- and liquid-state models may be extended to plasmas, leading to a consistent treatment of the high-temperature fluid phase.

In solid-state physics, quite accurate methods do exist to construct pair interactions for simple metals.[11-14] The case of more complex systems, such as transition metals, is less clear: the question arises as to whether two-body interactions are really relevant and, if they are, how to construct them in a physically transparent way.[15,16] Much less has been done in plasmas, even for systems having a simple electronic structure. A major difficulty is that the ionization state Z^* changes with temperature and density. The definition of Z^* itself is subject to controversy because this quantity is not the eigenvalue of any operator; Z^* may be in fact intuitively thought of as a number of electrons responding to external perturbation. Obviously, a given material is never "simple" (in the sense of "simple metal") for all densities $\bar{\rho}$ and temperatures T: there are domains of $\bar{\rho}$ and T where electron states evolve continuously from bound to resonant scattering states,[17] making the definition of Z^* somewhat ambiguous (in these domains, the plasma behaves more or less like a transition metal). Finally, there is a lack of reference calculations and experimental information allowing the test of the plasma $\phi(R)$ and $g(R)$.

In the present work, we assume the possibility of using the approach commonly adopted for liquid simple metals[10] at least in specific regimes of density and temperatures to be defined. This approach leads to dividing the free energy into an electronic contribution and an ionic contribution. The electronic contribution does not depend on the ionic positions and may be calculated using "single-ion" quantities. The ionic part is the free energy of a one-component system of ions interacting through a screened pair potential. Such a decomposition implies the adiabatic approximation (electronic time scale are much smaller than ionic ones) and is straightforwardly obtained in the weak model-potential perturbation (MPP) theory[10] and the neutral-pseudoatom (NPA) theory that does not require the fitting of parameters and provides fully nonlinear core and valence electron densities.[18]

The NPA theory has been successfully applied to simple metals at zero temperature and in very small ranges of density where Z^* is well defined and constant. Here we shall construct the NPA for finite temperatures with the help of the Mermin-Kohn-Sham[19,20] equations. Using the NPA electron density, we shall compute the electronic part of the free energy and extend the calculation of the ion-ion pair interaction ϕ to cases of $\bar{\rho}$ and T-dependent ionizations. Finally, by performing a coupling-constant integration, the ionic part of the free energy will be calculated, leading to the total free energy of the plasma.

The paper is organized as follows. The main features of the NPA theory are summarized in Sec. II where results for beryllium and aluminum metal at zero temperature and densities in the range of constant normal valence are also shown. Section III is devoted to higher densities on the $T=0$ isotherm; in this range of densities, the core states begin to overlap, and the definition of an effective valence Z^* (i.e., ionization state due to high pressure) is proposed, as well as that of the density profile (i.e., free-electron density) associated with it. With these quantities the total energy of the metal is computed as a function of the metal density $\bar{\rho}$ and compared with results of band structure calculations, which provide accurate reference energy curves $E(\bar{\rho})$. By doing so, we are able to propose and test a definition of Z^* in terms of the NPA bound and scattering electron densities. This definition is expected to be transferable to finite temperatures since there is no reason to believe that the delocalization of the average electron-density profile due to temperature behaves differently, with respect to Z^*, from that due to pressure effects. Various results relating to ionization Z^*, pair interaction, and equation of state at high densities in Be and Al are shown. The range of densities that can be dealt with in this model is discussed. Temperature effects are treated in Sec. IV where the calculation of the ion-ion contribution to the free energy is explicitly set out. Numerical results are presented and discussed. Finally, concluding remarks and guidelines for future work in the field are given in Sec. V.

II. NEUTRAL-PSEUDOATOM METHOD UNDER NORMAL CONDITIONS

The neutral-pseudoatom method was proposed first by Ziman,[21] and then extensively used by Dagens.[18,22,23] Its philosophy is the same as that of the pseudopotential method,[24] and so is its domain of applicability. In conjunction with density-functional theory (DFT),[19] it is entirely *a priori* and has the advantage of handling "true" densities instead of pseudodensities.

A. NPA densities

The NPA was, in its original version at zero temperature, applied to metallic systems where a clear distinction between non-overlapping core states and valence states is possible, i.e., to "simple metals." The density in the metal is assumed to be accurately given by a superposition of single site, structure independent, and localized densities $\Delta n(r)$, so that

$$n(\mathbf{r})=\sum_i \Delta n(\mathbf{r}-\mathbf{R}_i) . \tag{1}$$

Δn includes a core bound contribution n_b and a contribution from valence free states Δn_f

$$\Delta n(\mathbf{r})=n_b(\mathbf{r})+\Delta n_f(r) . \tag{2}$$

The superposition approximation is quite common in condensed-matter physics. For instance, the recent formulation of "embedding theories" in an effective medium[25–27] also makes use of it.

It is worth noting first that Eq. (1) is consistent with the binary character of interatomic forces and, hence, is perfectly compatible with the subsequent analysis of the total energy in terms of pair interactions.[28] It is assumed that there is no ambiguity in the valence (ionization) Z^* of the metal:

$$Z^*=Z-\int_\infty n_b(r)d\mathbf{r}=Z-\int_\Omega n_b(r)d\mathbf{r} , \tag{3}$$

with Z the nucleus charge. The last equality on the right-hand side is a consequence of the perfect localization of the core states within the atomic sphere volume Ω. Clearly, the free-electron density satisfies

$$\int_\infty \Delta n_f(r)d\mathbf{r}=Z^* . \tag{4}$$

The total external potential V_{ext} acting on the electrons is

$$V_{\text{ext}}=-\frac{1}{r}\circ\left[\sum_i Z\delta_i\right] , \tag{5}$$

where $\circ$ represents "convolution product," and δ_i is a delta function centered on site i. The basic idea of the theory is to treat separately, site by site, the various terms in Eq. (5). But the potential $-1/r\circ Z\delta$ is a "strong scatterer," having a Friedel sum equal to Z^* (we consider the Friedel sum as being zero at the bottom of the valence band), and displaces a free-electron density normalized to Z^* electrons. It has been shown that this results in a poor convergence of the multicenter expansion of the kinetic energy-functional $T[\sum_i \Delta n_i]$, which is necessary for calculating the total energy of the metal.[29] Such an expansion would have a much faster convergence if the overlapping part of Δn were to integrate to zero, i.e., if the external potential associated with it were to be a weak-scattering potential (Friedel sum equal to zero). To overcome this difficulty, the NPA method introduces the following external potential:

$$V^*_{\text{ext}}=\frac{1}{r}\circ\left[\sum_i -Z\delta_i+\sum_i \nu_i-\bar{n}\right] , \tag{6}$$

where $\bar{n}$ is the average free electron density in the metal

$$\bar{n}=\frac{Z^*}{\Omega}=Z^*\bar{\rho} \tag{7}$$

($\bar{\rho}$ is the material density) and ν_i is the so-called "auxiliary screening function." The auxiliary screening function is chosen in such a way that $\sum_i \nu_i-\bar{n}$ is as small as possible, and its integral must be Z^*. It is approximately that part of the uniform background $\bar{n}$ which can be attributed to a single ion. To some extent, it is arbitrary. In our applications, we chose the simplest form, i.e., that of a spherical cavity. Other choices where $\nu(r)$ is a continuous function of r instead of a step function have been considered.[18,23] The total electron density in the external potential V^*_{ext} for the "auxiliary" system is

$$n^*=\bar{n}+\sum_i \Delta n_i^* . \tag{8}$$

The total screened potential associated with Eqs. (6) and (8) is

$$V^* = \frac{1}{r} \circ \sum_i (-Z\delta_i + \nu_i + \Delta n_i^*) \tag{9a}$$

$$= \sum_i V_i^* \ . \tag{9b}$$

Due to the use of the screening function ν, the Friedel sum associated with V_i^* and Δn_i^* is zero. The NPA is thus a weak scatterer and the superposition approximation of the single site densities in the metal is expected to be quite a good approximation. This minimum scattering property also allows us to use a cluster-type expansion of the total energy, as will be seen in the following paragraph. The calculation of the NPA consists in solving self-consistently the DFT equations for a single potential V_i^* and a single density Δn_i^*. The reduction of the multiple-scattering problem to a single-scattering problem is the characteristic feature of the theory of simple metals. Now the difference between the exact $V_{\rm ext}$ and its approximation $V_{\rm ext}^*$ is treated in linear response theory, giving a density change

$$\delta n(\mathbf{r}) = \sum_i m(\mathbf{r} - \mathbf{R}_i) - \bar{n} \ . \tag{10}$$

The exact density response function of the auxiliary system would be rather difficult to calculate. We can remark that $\bar{n} - \sum_i \nu_i$ is nonzero only near the surface of the Wigner-Seitz cells, precisely where the electron density is most uniform. So we write

$$m(r) = \frac{-1}{(2\pi)^3} \int d\mathbf{q} \frac{\pi_0(q)}{\epsilon(q)} \frac{4\pi}{q^2} \nu(q) e^{-i\mathbf{q}\cdot\mathbf{r}} \ , \tag{11}$$

where $\pi_0(q)$ is the uniform electron-gas density response function, $\epsilon(q)$ the dielectric constant, including local-field corrections, and $\nu(q)$ the Fourier transform of the screening function $\nu(r)$; $m(r)$ carries a charge equal to Z^*. Collecting Eqs. (8) and (10), one finds that the "true" density of the metal is, from Eq. (1),

$$n(\mathbf{r}) = \sum_i (\Delta n_i^* + m_i) \tag{12a}$$

$$= \sum_i [n_b(\mathbf{r} - \mathbf{R}_i) + \Delta n_f^*(\mathbf{r} - \mathbf{R}_i) + m(\mathbf{r} - \mathbf{R}_i)] \ , \tag{12b}$$

since the bound density is insensitive to the first-order change $V_{\rm ext} - V_{\rm ext}^*$.

B. Total energy expansion

To calculate the total energy of the system at zero temperature, we determine first the energy of the "auxiliary" system in the external potential $V_{\rm ext}^*$. Then we add the contribution due to $V_{\rm ext} - V_{\rm ext}^*$ in second-order perturbation theory.

The electron density n^* of the auxiliary system is given in Eq. (8). Let us consider the functional $G[n^*]$ including the kinetic and exchange-and-correlation energies. It has been shown that this functional may be rewritten as an infinite expansion:[30]

$$G\left[\bar{n} + \sum_i \Delta n_i^*\right] = G[\bar{n}] + \sum_i G_i + \tfrac{1}{2}\sum_{i,j}' G_{ij} + \frac{1}{3!}\sum_{i,j,k}'' G_{ijk} + \cdots \ , \tag{13}$$

$$G_i = G[\bar{n} + \Delta n_i^*] - G[\bar{n}] \ , \tag{14a}$$

$$G_{ij} = G[\bar{n} + \Delta n_i^* + \Delta n_j^*] - G_i - G_j - G[\bar{n}] \ . \tag{14b}$$

G_{ij} goes to zero for pairs of sites which are far apart and, similarly, G_{ijk} vanishes when the distance between any two of three sites i,j,k is very large. It should be noted that such an expansion does not require Δn^* to be small every where compared with $\bar{n}$. For simple metals, the expansion is truncated after the second-order term, consistently with the two-body interaction picture. The electrostatic interaction energy U

$$U = V_{\rm ext}^* \cdot \sum_i (\Delta n_i^* + \nu_i) + \tfrac{1}{2}\sum_{i,j} (\Delta n_i^* + \nu_i) \cdot \frac{1}{r} \circ (\Delta n_j^* + \nu_j) + \tfrac{1}{2}\sum_{i,j}' \frac{Z^2}{R_{ij}} \tag{15}$$

is straightforwardly added to $G[n^*]$. In Eq. (15), we have used the dot as a shorthand notation for the scalar product in direct space, i.e.,

$$f \cdot g = \int d\mathbf{r} \, f(\mathbf{r}) g(\mathbf{r}) \ .$$

Finally, the second-order perturbation energy associated with $V_{\rm ext} - V_{\rm ext}^*$ is

$$\delta E = (n^* + \tfrac{1}{2}\delta n) \cdot \frac{1}{r} \circ \left[\bar{n} - \sum_i \nu_i\right] , \tag{16}$$

where δn is given in Eq. (10). The contribution depending on δn may be easily calculated in reciprocal space. After some tedious manipulations, which we shall not reproduce here in detail, the total energy of the system is obtained as follows:

$$E = G[\bar{n}] + N\Delta E_i + N(\bar{n} - \nu_i) \cdot V_i^* + \tfrac{1}{2} N \nu_i \cdot \frac{1}{r} \circ (\nu_i - m_i) - \tfrac{1}{2} N Z^* 4\pi \bar{n} \sigma + \tfrac{1}{2}\sum_{ij}' \phi_{ij} \ . \tag{17}$$

The meaning of the various terms in Eq. (17) is the following. The first one is the energy of a uniform interacting electron gas of density $\bar{n}$, the number of electrons per volume $\Omega = \frac{4}{3}\pi R^3$ (R is the average atomic radius of the material) being Z^*:

$$G[\bar{n}] = NZ^*[\tfrac{3}{10}k_F^2 + \varepsilon_{\rm xc}(\bar{n})] = NE_0 \ , \tag{18}$$

with N the number of atoms, k_F the Fermi momentum, and $\varepsilon_{\rm xc}(\bar{n})$ the exchange-and-correlation energy density. The second term ΔE_i is just the energy required to embed a single NPA (with external charge $-Z\delta_0 + \nu_0$ at origin) in the jellium. This energy is the result of a full self-consistent DFT calculation. Such calculations are now quite standard in solid-state physics, and often used for the study of impurities, vacancies, etc.[31,32] The three following terms are single-site terms (the subscript indicates that the quantities ν, V^*, and m refer to one single site

which can be chosen at origin, i.e., $i=0$) brought by the corrections to the NPA. The first of these terms depends on the single-site screened Coulomb potential and is easily calculated as

$$(\bar{n}-\nu_0)\cdot V_0^* = \int_R^\infty \bar{n} 4\pi r^2 dr\, V_0^* \ .$$

The two other terms are independent of the NPA density profile; they are functions of $\bar{n}$ and Z^* only. The quantity σ, which has the dimension of a surface, is defined by

$$\sigma = \frac{1}{\lambda_{\rm TF}^2} - \frac{1}{4k_{\rm xc}^2} \ , \tag{19a}$$

where $\lambda_{\rm TF}$ is the Thomas-Fermi screening constant, i.e., $\lambda_{\rm TF}^2 = 4k_F/\pi$, and

$$\frac{1}{4k_{\rm xc}^2} = \lim_{q\to 0}\frac{g(q)}{q^2} = -\frac{1}{4\pi}\frac{dV_{\rm xc}(\bar{n})}{d\bar{n}} \ , \tag{19b}$$

where $g(q)$ is the local-field factor entering the dielectric constant $\epsilon(q)$

$$\epsilon(q) = 1 - \frac{4\pi}{q^2}[1-g(q)]\pi_0(q) \ . \tag{20}$$

$g(q)$ is evaluated in the local-density approximations (LDA) for the exchange-correlation effects, and is thus proportional to q^2 and to the derivative of the exchange-correlation potential with respect to density, i.e., $dV_{\rm xc}(\bar{n})/d\bar{n}$. In our applications, we used various approximations for these exchange-correlation functionals, as will be shown later. Finally, the last term in Eq. (17) is the only one which depends on structure. It is expressed in terms of the pair interaction which has the following formal expression:

$$\phi(R_{ij}) = G_{ij} + (-Z\delta_i + \Delta n_i^*)\cdot\frac{1}{r}\circ(-Z\delta_j + \Delta n_j^*) - \nu_i\cdot\frac{1}{r}\circ m_j \tag{21}$$

where G_{ij} is the two-center contribution to the kinetic plus exchange-and-correlation energy in the auxiliary system, as defined in Eq. (14b). As the explicit form of G is unknown, the calculation of $\phi(R_{ij})$ is subject to further simplifications described below.

C. Calculation of the pair interaction

The density associated with every ion in the metal is, Eq. (11b),

$$\Delta n = n_b + \Delta n_f^* + m \ .$$

This density is expected to be much better than the one which would result from a linear response to a model potential for the ion, because it is calculated by solving the Kohn-Sham equations and is thus valid to all orders in the potential.

It has been proven elsewhere that the pair interaction $\phi(R_{ij})$ can be expressed as a surface integral in the symmetry plane between ions located at $\mathbf{R}_i$ and $\mathbf{R}_j$. The integrand depends on the pressure tensor and Maxwell stress tensor, calculable with the wave functions and the potential, for distances larger than $R_{ij}/2$ only.[17] Thus the ion-pair interaction does not depend significantly, in the region of space where it is useful, that is outside the ionic cores, on the shape of the density inside the cores. In other words, the pair interaction will not be affected if we change Δn within the core, say for radii smaller than a core radius R_c. The advantage of making such a change is that, by a suitable smoothing of Δn_f^*, one can get rid of the inner-shell oscillations and obtain a Fourier transform having a much better convergence at large q. Consequently, we shall work with the modified density Δn_m^*:

$$\Delta n_m^* = \begin{cases} \Delta n_f^* & \text{if } r \geq R_c \quad (22a) \\ A + Br^2 + Cr^3 & \text{if } r \leq R_c \quad (22b) \end{cases}$$

where A, B and C are constants chosen in order to preserve continuity of Δn_m^* and of its derivative at $r=R_c$, and keep the correct zero integrated charge of Δn_f^*.

Now, it is assumed that there exists a local model potential that gives Δn_m^* in linear response.[14] If it is the case, this model potential is

$$w(q) = \frac{\epsilon(q)}{\pi_0(q)}\Delta n_m^*(q) \ , \tag{23}$$

and we can check that the assumption is sound if $w(q)q^2/4\pi Z^*$ is not significantly larger than 1 for any q. Introducing this approximation in Eq. (21), and the corresponding DFT equation for G_{ij}

$$G_{ij} + w_i\cdot\Delta n_m^*(\mathbf{r}-\mathbf{R}_j) + \Delta n_m^*(\mathbf{r}-\mathbf{R}_i)\cdot\frac{1}{r}\circ\Delta n_m^*(\mathbf{r}-\mathbf{R}_j) = 0$$

allows the practical calculation of ϕ. We get, with $v=4\pi/q^2$,

$$\phi(q) = (Z^*)^2 v + \frac{\pi_0(q)}{\epsilon(q)}[w(q)-v\nu(q)]^2 \ . \tag{24}$$

In our numerical calculations, we determined the core radius R_c by requiring that

$$n_b(R_c) + \Delta n_f^*(R_c) = \lambda\bar{n} \ ,$$

i.e., the total NPA density at R_c is a fraction of the background density $\bar{n}$. We checked that a reasonable variation of λ from 0.5 to 1.0 does not affect the results. All the Fourier transforms were calculated using the fast-Fourier-transform technique with a 4096-point mesh. The contribution of the long-range tail (Friedel oscillations) of the density was carefully taken into account via an analytical correction in $\Delta n_m^*(q)$. Also, in computing the pair interaction in direct space, we replaced Eq. (24) by the equivalent one:

$$\phi(r) = \frac{(Z^*)^2}{r}\operatorname{erfc}(\alpha r) + \frac{1}{(2\pi)^3}\int d\mathbf{q}\, e^{i\mathbf{q}\cdot\mathbf{r}}\left[\frac{\pi_0}{\epsilon}(w-v\nu)^2 + (Z^*)^2 v\exp\left[\frac{-q^2}{4\alpha^2}\right]\right] , \tag{25}$$

which avoids cancellation of large-r Coulomb tails obtained in a straightforward use of Eq. (24). Finally, the contribution of the pair interaction to the energy

$$NE_{\text{pair}} = \tfrac{1}{2}\sum_{i,j}{}' \phi(R_{ij}) \tag{26}$$

was calculated on the fcc lattice up to 100 shells of neighbors and the remaining contribution was treated by means of a continuous integration.

D. Results

We applied the method to Be and Al for which we have a large number of reference calculations. In the case of Be, we used the Nozières-Pines exchange-correlation formula in order to compare with band-structure (BS) calculations done with the same exchange-correlation choice in the linear muffin-tin orbital (LMTO) technique.[33,34] At normal density ($R = 2.315\,16$ a.u.), we found a total energy of -29.146 Ry, to compare with -29.167 in the LMTO-BS model.[33] For Al, also at the reference density ($R = 2.9907$ a.u.), the present work gives -480.952 Ry instead of -480.943 Ry using the augmented plane waves (APW) band structure method with the Kohn-Sham (KS) exchange-correlation formula.[35] In Figs. 1 and 2 we extend the comparison to higher densities in a range where Z^* does not change ($Z^* = 2$ for Be and 3 for Al). In these figures, the BS curves have been shifted by a constant energy in order to bring the minima to coincidence. Thus we can see more directly the deviations due to increasing the density. The results are slightly better for Al. We think that the largest deviation in Be is due to more important BS effects where there is a pronounced depletion in the density of electronic states at the Fermi level because the $2s$ shell is filled. But the overall agreement is quite satisfactory when one notes the very different character of the methods employed.

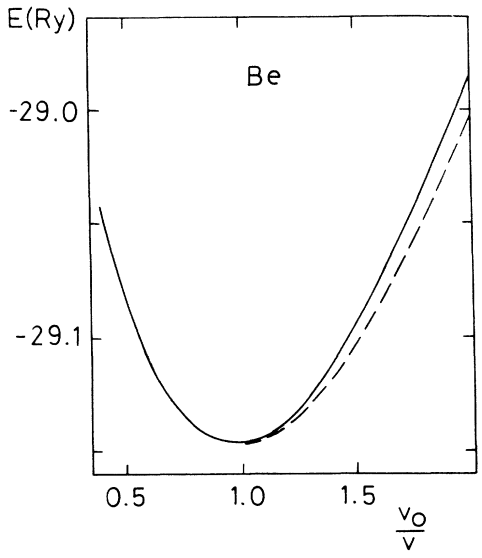

FIG. 1. Variation of the total energy E with compression c for Be, in the vicinity of equilibrium, at zero temperature. $Z^* = 2$ everywhere in this region.

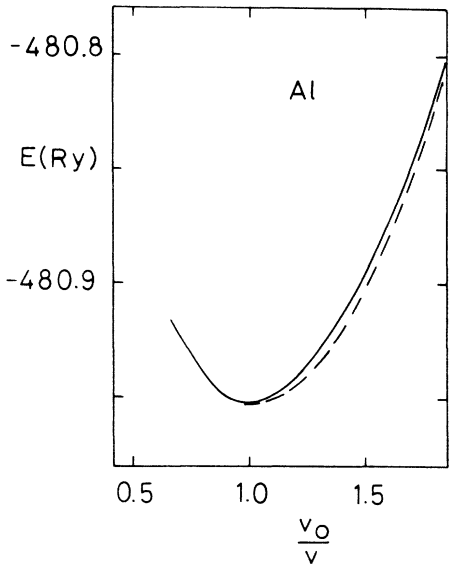

FIG. 2. Same as Fig. 1, but for Al $Z^* = 3$.

III. EXTENSION TO VERY HIGH DENSITIES

In this section, we consider the phenomenon of "pressure ionization." When $\bar{\rho}$ increases enough, the core levels centered on different sites begin to overlap and to form energy bands.[17] Part of the corresponding electron density is expected to participate in the response of the system to external perturbations. As a consequence of this effect, Z^* increases. This induces important variations in the physical properties of the metal. It has been shown that these properties, such as the total binding energy E, the pressure P, and its derivative $dP/d\bar{\rho}$ are continuous when a bound state is pressure ionized (i.e., goes into the continuous spectrum).[17] The NPA total electron density Δn^* also is continuous, not Δn_f^* alone.[36] If the density n_b of the bound states has a very long slowly decreasing tail (because the highest level is very shallow), this tail is canceled in Δn^*, for large r, by an opposite contribution in Δn_b^*. These considerations prove that Z^* must be related to the total density (at least for large distances) and not to the scattering states density only.

For this reason, we propose the following sharing of the electron density:

$$\begin{aligned}\Delta n^* &= n_b + \Delta n_f^* \\ &= f n_b + (1-f) n_b + \Delta n_f^* \ .\end{aligned} \tag{27}$$

In Eq. (27), f is a "cutting function" defined by

$$f = \frac{1+e^{-1/\mu}}{1+e^{(r-R)/\mu R}} \ , \tag{28}$$

which is 1 inside the atomic sphere (radius R), 0 outside, and decreases very fast from 1 to 0 around the sphere radius. In all our calculations, we used the value $\mu = 0.05$; f was never modified and not used for any fitting purpose. The advantage of using this f instead of a pure step function is that it perturbs much less the large q behavior of the density Fourier transform. Now, we write

$$n_b' = f n_b \ , \tag{29a}$$

$$(\Delta n_f^*)' = (1-f) n_b + \Delta n_f^* \ , \tag{29b}$$

defining the "new" rigid bound states density n_b' and the "new" density of responding free states $(\Delta n_f^*)'$. Obviously, the original definitions are recovered if there is no core overlap. The ionization associated with these definitions is

$$Z^* = Z - \int_\infty n_b' d\mathbf{r} \ , \tag{30}$$

and, as the neutrality condition

$$Z = Z^* + \int_\infty \Delta n \, d\mathbf{r} \tag{31}$$

still holds, it is easy to establish that

$$0 = \int_\infty (\Delta n_f^*)' d\mathbf{r} \ ,$$

i.e., the integrated charge of the responding electron density remains equal to zero.

A correct calculation of Z^* is crucial because the material density $\bar{\rho} = \bar{n}/Z^*$ is proportional to its inverse. Errors in Z^* would prevent accurate reproduction of the BS energy curves. This point is illustrated for Be in Figs. 3 and 4. We see clearly that our prescription for identifying the density-dependent Z^* allows us to get good agreement with the BS results[33,34] up to compression $c = 40$ approximately. On the contrary, if Z^* is calculated from Eq. (4) [that is, with $f = 1$ in Eq. (29a)], leading to $Z^* = 2$, the energy curve is much too low for compression higher than $c = 10$, as can be seen in Fig. 4. The results also show that our definition of Z^* leads to an important deviation with respect to the BS energy for $c \geq 40$. The reason is the following. At $c = 40$, the NPA $1s$ bound state goes into the continuum. For c slightly lower, it is easily established that the $1s$ electron density, at large r where the screened total potential is negligible, is of the form

$$n = \frac{A^2}{r^2} \exp(-2\sqrt{-\varepsilon} r) \ . \tag{32}$$

If R_l is the value of the atomic sphere radius where the $1s$ state disappears, one can write its eigenvalue

$$\varepsilon = a(R_l - R) \ , \tag{33}$$

where a is some constant. As the $1s$ state is normalized, A^2 must be proportional to $(R_l - R)^{1/2}$, so that just below the $1s$ ionization limit, the value of Z^* (proportional to the charge of the $1s$ state outside the sphere) is of the form

$$Z^* \simeq 2\{1 + \exp[-2R\sqrt{a(R - R_l)}]\} \tag{34}$$

(in this qualitative derivation, we disregard the effect of the cutting function f, i.e., we take $f = 1$). Consequently, the ionization Z^* would have an infinite slope $dZ^*/d\bar{\rho}$ at the threshold. This tendency is shown in Fig. 5. In fact, this behavior is physically incorrect and would induce an anomalous density dependence of the thermodynamic functions. It reflects clearly the limit of validity of the model: when the overlap of the core states is too large, the description of the plasma in terms of rigid single-site

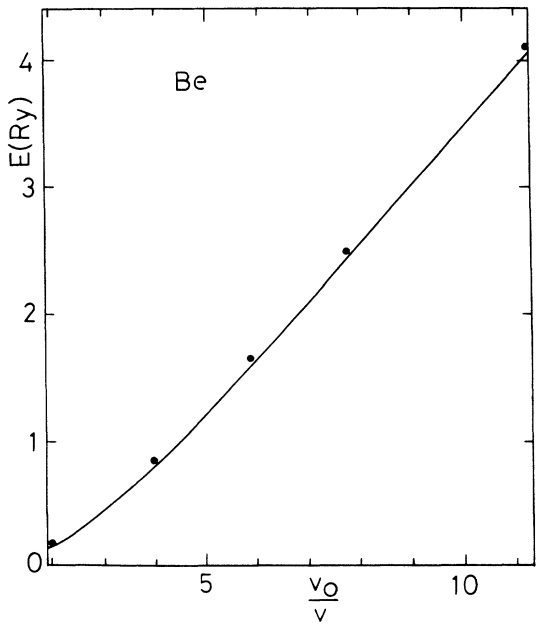

FIG. 3. Total energy as a function of compression for Be, in the high-density region. The value of energy at $c = 1$ has been subtracted. Solid curve, band-structure calculations (Refs. 33 and 34); Dots, results of the present work.

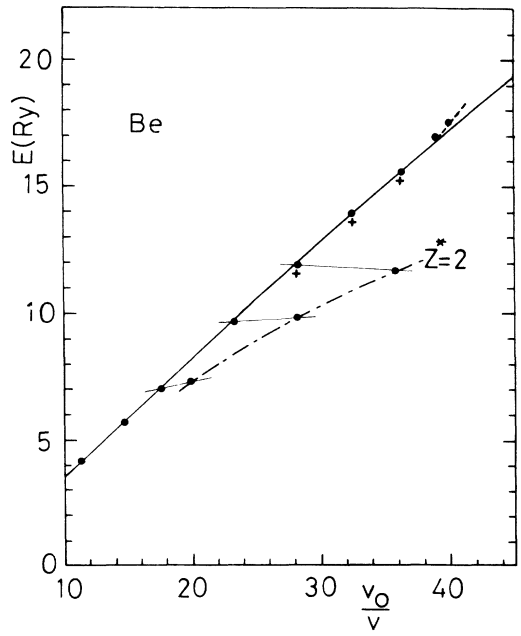

FIG. 4. Total energy in Be, in the very-high-density range. E is measured with respect to its minimum at $c = 1$. Solid curve represents the band structure calculations (Refs. 33 and 34). ●, present model; +, with terms beyond the NPA in linear response for ions having the charge Z^* calculated in the present model; —·—·—, calculation in the present model, but with a frozen $Z^* = 2$ ionization (no pressure ionization). For compression higher than 40, the results of the present model begin to diverge from the solid curve.

densities becomes inadequate. The formation of non-free-electron-like energy bands cannot be accounted for in our simple picture. Band-structure calculations for Be at high densities[34] show that the gap between the $1s$ band and the upper ones closes at $c=50$ approximately. This allows us to present in Fig. 5 a reasonable estimate of Z^* above $c=40$ and up to $c=50$.

At compression 40, the pressure in Be reaches an enormous value of about 1800 Mb; it is expected that the statistical models of condensed matter (Thomas-Fermi with possible density-gradient corrections and exchange-correlation corrections) would become reliable, so that more detailed models are perhaps not needed at higher compressions. Even at $c=40$, the density parameter r_s remains too large (its value is $r_s=0.47$) to justify a complete treatment based on linear screening of the bare ions (such a treatment is expected to be valid if $r_s \leq 0.1$). Nevertheless, we have also made the following calculation: we calculated the terms which go beyond the NPA in Eq. (17) (i.e., terms different from $G[\bar{n}]+N\Delta E_i$) in linear response, including the external potential $-1/r_0 \sum_i Z^* \delta_i$, Z^* having the value calculated within the present scheme. The results are shown in Fig. 4; the total energies calculated this way are lower, but still represent a sensible approximation.

In Fig. 6, we display the variation of the pair interaction energy E_{pair}, Eq. (26), as a function of compression. We also compare it in the range $1 \leq c \leq 40$ to results obtained with a fixed valence $Z^*=2$, or within linear response theory with ions of charge Z^*. This comparison shows strong discrepancies between the two latter approximations and the full theory. The curve shown for c above the $1s$ ionization threshold, obtained in linear theory with $Z^*=4$, seems to be able to provide a useful extrapolation at very high compressions, say $c > 60$.

Pair interactions at high compression $c=36$ are shown in Fig. 7. Both curves correspond to the NPA value of Z^* ($=2.86$), but one is obtained using the linear response density. The latter leads to a lower $\phi(r)$ and thus to a smaller pair energy.

We have applied the method to Al also. In this metal, Z^* begins to differ significantly from its normal value ($Z^*=3$) at $c=5$, when the $2p$ wave functions start overlapping. Our definition of Z^* works quite well up to $c=15$ approximately, as shown in Fig. 8, where the

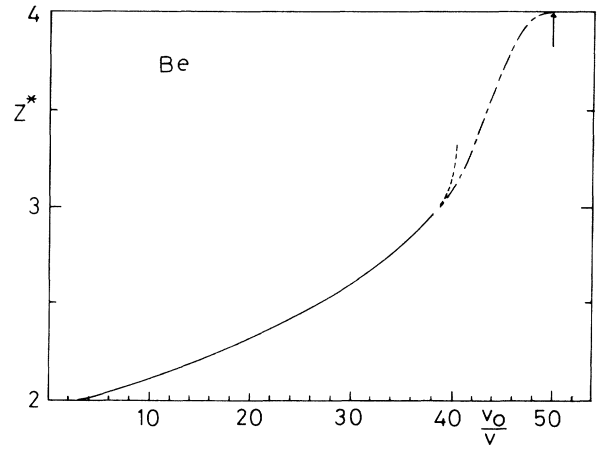

FIG. 5. Average ionization Z^* in Be at $T=0$. The ionization of the $1s$ level calculated in the present model causes a spurious behavior of Z^* around $c=40$. Band-structure calculations indicate that the gap between the $1s$ and $2s$ bands closes at $c=50$. The dot-dashed curve is a reasonable guess between $c=40$ and 50.

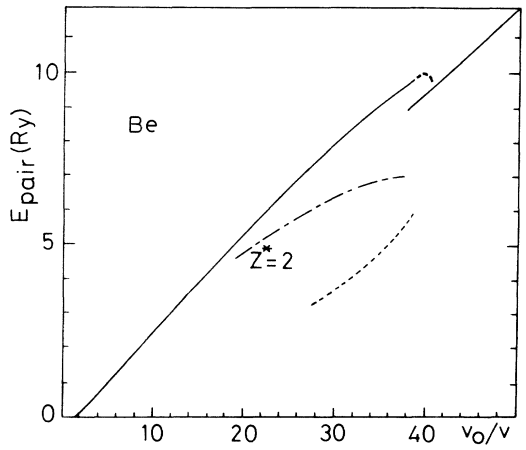

FIG. 6. Pair-interaction energy in Be at $T=0$. Solid curve for $c \leq 40$, present model, which fails around $c=40$; solid curve for $c \geq 40$, calculation in linear response with bare ions of charge $Z^*=Z=4$; dot-dashed curve represents the calculation in the present model, but with Z^* frozen at its "normal" value; dotted curve represents the calculation in linear response for bare ions with the charge Z^* calculated in the present model.

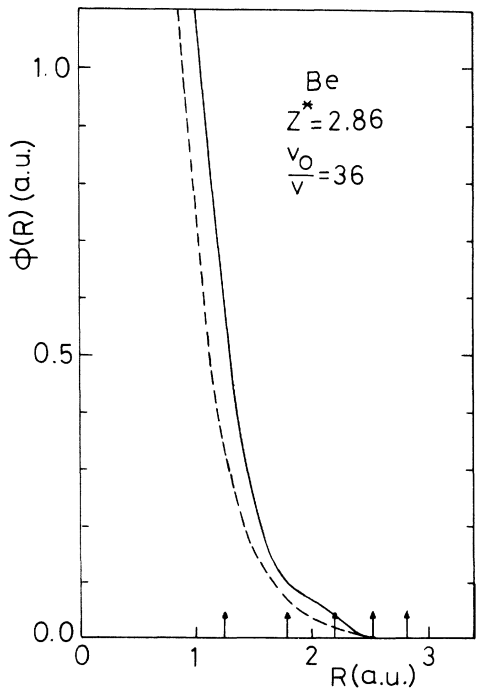

FIG. 7. Pair interaction in Be at a very high compression $c=36$. Solid curve, present model; dotted curve, the density Δn^* is obtained from linear response with Z^* of the present model.

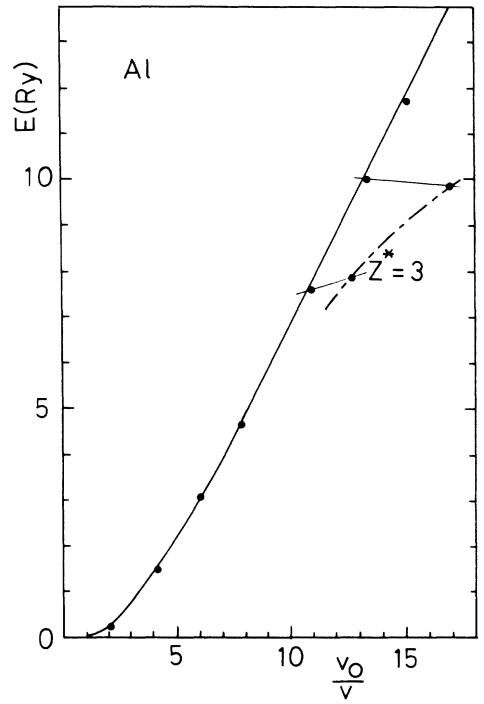

FIG. 8. Total energy in aluminum, at $T=0$, as a function of compression. Solid curve, band structure (APW) calculation; dots, present model; dot-dashed curve, present model with Z^* frozen at its "normal" value $Z^*=3$. Points that are linked together correspond to the same electron density $\bar{n}$.

agreement between our calculated energies and those of the BS calculation of McMahan and Ross[35] is nearly perfect. Also, as in the case of Be, a calculation at constant $Z^*=3$ would give very poor results for $c>5$. In Fig. 9, we display the evolution with respect to density of the bound charge (i.e., the amount of charge inside the atomic sphere) for the $2s$ and $2p$ bound states. We see that the $2p$ state goes into the continuum at $c=16$, but for this symmetry, the charge remains finite, contrary to the case of s symmetry. The reason is that the asymptotic behavior of a p wave function at threshold is similar to r^{-2}, so that the density goes like r^{-4} and is thus normalizable. For compressions higher than the limit, a resonant scattering state is found in the continuum. Its width w decreases when $\bar{\rho}$ continues to increase. A "relevant" parameter to characterize this resonance could be[15]

$$x=\frac{w}{\varepsilon_F},$$

the ratio of the width to the Fermi energy. As long as the energy ε_r of the resonant state is lower than ε_F, and x is much smaller than 1, the resonant state keeps a bound character, at least for distances not too large. Obviously, this resonant state contributes to some extent to the total ion bound charge and must not be counted as a pure free state (otherwise, Z^* would have a discontinuity at threshold). The appearance of resonant states indicates the limit of the domain of applicability of the present technique. The treatment of metals where such states do exist is a difficult problem in pseudopotential theory. The models that have been proposed up to now, for instance for transition metals,[15,16] lead to complex calculations, which are outside the scope of the present study. Furthermore, it seems that there is no guarantee that the pair-interaction picture is correct in these systems. Thus we shall not push our model to densities where resonances do occur. For plasmas, we shall restrict its application to $\bar{\rho}$-T regimes where the plasma may be considered as "simple," in the sense of "simple metals," i.e., where the continuum states are mainly free-electron-like. Fortunately, the width of the resonances is increased by the temperature so that the problem may become much less crucial in high-temperature plasmas.

In Fig. 10, we display the evolution of Z^* with compression up to $c=16$; comparison with the ionization obtained in a standard manner in Thomas-Fermi theory is also shown, with considerable discrepancies. The pair energy E_{pair} is shown in Fig. 11, and the pair interaction $\phi(R)$ at normal density in Fig. 12. This interaction was calculated with Kohn-Sham exchange (no correlation) in order to be consistent with the BS calculations used as a reference for Al.[39] We checked that our calculated $\phi(R)$

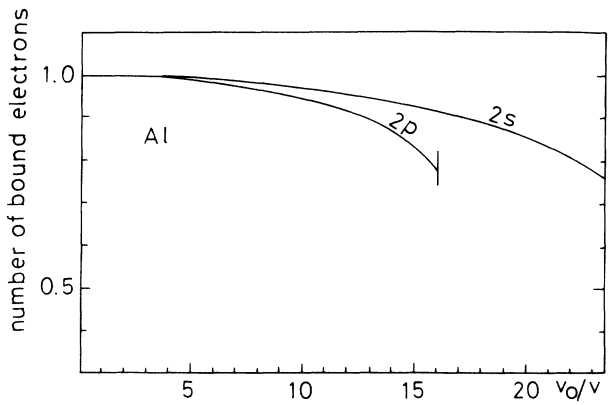

FIG. 9. Electron bound charge contained in the atomic sphere, for the $2s$ and $2p$ states of Al, as a function of compression at $T=0$. The $2p$ state is pressure ionized at $c=16$.

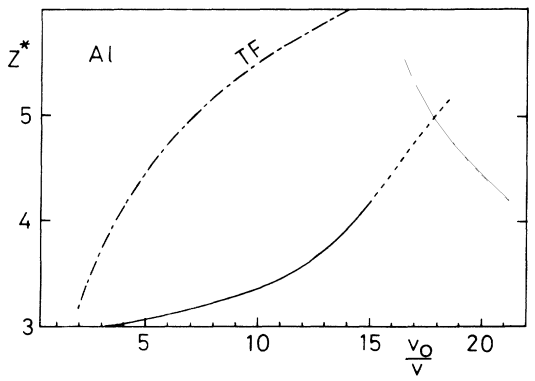

FIG. 10. Ionization Z^* of Al, at $T=0$, as a function of compression. Also shown is the Thomas-Fermi ionization (dot-dashed curve). The latter is obtained as the product of the atomic volume by the Thomas-Fermi electron density on the surface of the atomic sphere.

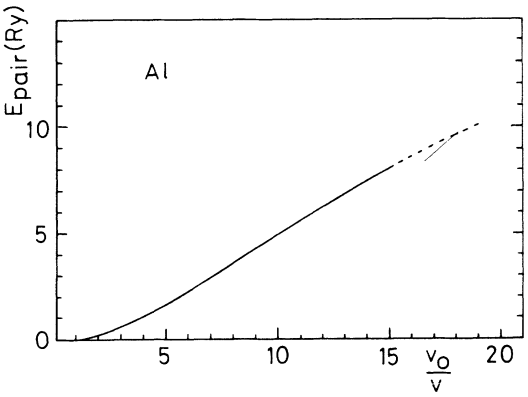

FIG. 11. Pair-interaction energy in Al at $T=0$.

comes into very good agreement with other similar calculations when correlation effects are added in the LDA.[12,14] The pair interaction at high density, $c=15$, is shown in Fig. 13, where it appears that the range of the potential is much shorter due to a stronger screening. Both curves are displayed in the region of r values where the first shells of neighbors are located.

The evidence from the results presented in this section lends support to our definition of Z^* in terms of the NPA bound and free densities, provided that the electronic structure of the condensed system remains simple. In this respect, the model can deal with partially delocalized s and p bound states, but cannot treat their complete transition to the continuum. The definition of Z^* can be

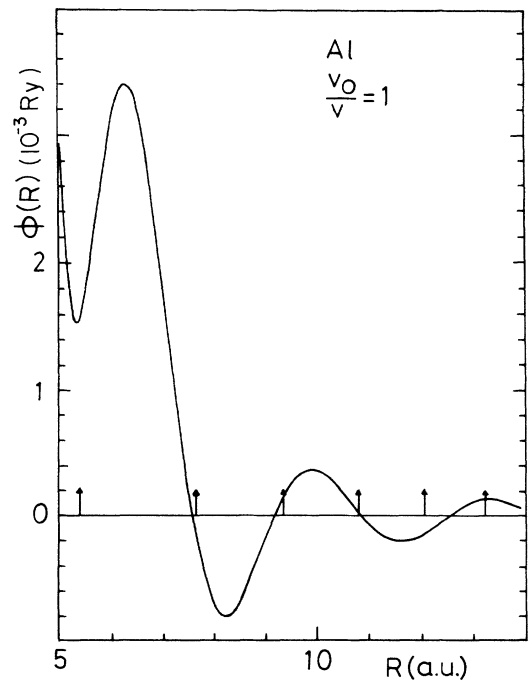

FIG. 12. Pair-interaction potential in Al at $T=0$, and for the reference density. The arrows indicate the positions of shells of atoms. KS exchange, no correlation.

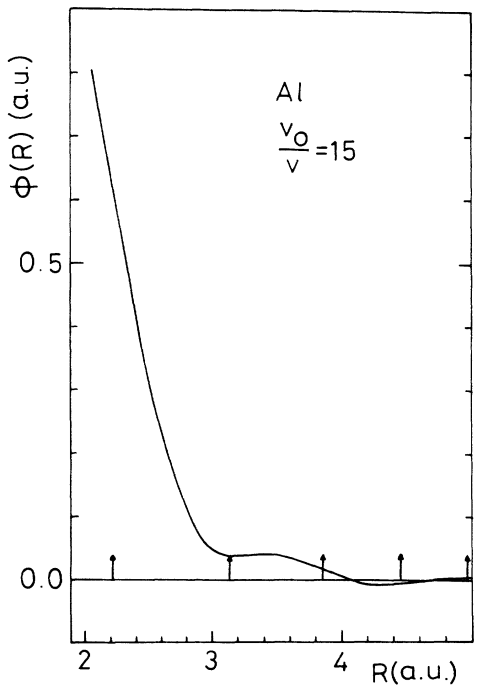

FIG. 13. Same as Fig. 12, but for compression $c=15$.

straightforwardly extended to any temperature. If the temperature is raised, at a density where the model works for $T=0$, there is no reason to believe that it will not be applicable since the DFT bound eigenvalues decrease, leading us to a more localized bound charge; the temperature effect is smooth at constant density. Even if new bound states do appear, their population will in general be small enough to avoid any sudden change in the electronic structure.

IV. HIGH-TEMPERATURE PLASMAS

A. Extension of the model to finite temperatures

Assuming that $\bar{\rho}$ and T are such that the plasma electronic structure is simple, there is no major difficulty in extending the DFT calculation of the NPA to finite temperature T. The Mernim-Kohn-Sham equations,[19,20] defining an "average" neutral pseudoatom, are solved self-consistently using techniques which are now standard.[37,38] We will not describe these numerical techniques in detail here, but only emphasize some points. At finite T, the free spectrum is no longer bounded by the maximum energy $\varepsilon_{\max}=\varepsilon_F$, the Fermi energy, but is infinite. Practically, we restrict the full quantum-mechanical calculation of the wave functions to energies lower than $\varepsilon_{\max}=\varepsilon_F+7kT$, and compute a correction for the remaining part of the spectrum using a restricted Thomas-Fermi (TF) approximation. The maximum orbital angular momentum $l_{\max}$ is still fixed to 10, but here also a correction for higher values of l is obtained in the TF approximation. Corrections to energies associated with these corrections to the electron density are also computed.

At finite temperatures, the basic thermodynamic function of the Mermin-Kohn-Sham scheme is the Helmholtz free energy F. Still using the superposition of densities given in Eq. (8), together with the cluster expansion truncated after second order term, Eqs. (13) and (14), the free energy is straightforwardly expressed similarly to Eq. (17), with $G[\bar{n}]=NF_0$ now being the free energy of the uniform interacting electron gas, and ΔF_i the free energy of embedding the NPA in the jellium of density $\bar{n}$, instead of ΔE_i. Of course, the response function to be used in the calculation of m and ϕ is now the RPA response function at finite temperature. The exchange-correlation effects are described by Ichimaru and Tanaka's analytic fit of $f_{xc}(\bar{n},T)$,[39,40] and the local field factor entering the dielectric constant is calculated consistently. The resulting pair interaction is now density and temperature dependent. The last term entering the finite-T counterpart of Eq. (17) is the free energy of the ionic component of the plasma, F_{pair}. The hypernetted-chain (HNC) equation is solved to obtain the pair correlation in the plasma. In the calculations reported here, no bridge term was included in the integral equation, but the effect of such a correction will be investigated in the future. Owing to the T dependence of ϕ, F_{pair} must be calculated using a coupling-constant integration. In the specific case of the pure HNC equation, such an integration may be avoided,[41] but it cannot in the case where corrections are included. In order to keep our numerical code as general as possible, we decided to actually perform this integration. Thus, for a given interaction $\phi(r;\bar{n},T)$, we solved the HNC equation with potentials $\lambda\phi$ for a number of values of λ in the range 0 to 1, each of them giving a pair correlation function $g(r;\lambda,\bar{n},T)$. Then, F_{pair} is, per ion,

$$F_{pair}(\bar{n},T)=\tfrac{1}{2}\bar{\rho}\int_0^1 d\lambda \int d\mathbf{r}\, g(r;\lambda,\bar{n},T)\phi(r;\bar{n},T) . \quad (35)$$

In practice we used ten values of λ between 0 and 1, following the law $\lambda=(n/10)^2$, $n=1,\ldots,10$.

For clarity in the analysis of the results, let us give the expression of the total Helmoltz free energy, collecting all the terms mentioned just above. Per ion, we have

$$F=F_0+\Delta F_i+F_c+F_{pair} , \quad (36)$$

with, as in Eqs. (17) and (19),

$$F_c=(\bar{n}-v_0)\cdot V_0^*+\tfrac{1}{2}v_0\cdot\frac{1}{r}\circ(v_0-m_0)-\tfrac{1}{2}Z^*4\pi n\sigma . \quad (37)$$

Numerical results for these terms are presented below.

B. Results

We performed calculations of the free energy of Be plasmas at compressions $c=1$ and 10 approximately, for temperatures up to 100 eV. In Tables I and II we give the results. These tables include neither the ideal part of the ionic free energy at finite T, nor the zero point motion energy at $T=0$. At normal material density (Table I), the electron density $\bar{n}$ is 0.038 48 a.u. and the Fermi temperature is 14.84 eV. As the temperature is increased at constant volume, $\bar{n}$ increases because Z^* does, so that $\bar{n}=0.068\,12$ a.u. at $T=100$ eV ($T_F=21.72$ eV). In this range of temperatures, the standard coupling parameter $\Gamma=(Z^*)^2/kTR$ goes from 18.81 for $T=2.5$ eV to $\Gamma=1.47$ for $T=100$ eV, covering a wide domain of strongly coupled plasmas. These quantities Z^* and Γ are displayed in Fig. 14. Looking at the various contributions to the free energy, we see that F_0 is that one which shows the largest amplitude of variation. Nevertheless, in the low-temperature range $T\le T_F$, it is clear that an accurate calculation of all the terms is required to get the correct total F, owing to cancellations between the various components. In Fig. 15, we show the pair interaction ϕ in Be at normal density and for $T=0$, 2.5, and 5.0 eV.

TABLE I. Free energy in Be at the reference density $\bar{\rho}_0=1.9436$ g cm^{-3} as a function of temperature. The electron density parameter is $r_s=1.837$ when $Z^*=2$. F_0 is the contribution of Z^* electrons in a uniform interacting electron gas. ΔF_i is the free energy for embedding the NPA. F_{pair} is the Helmholtz free energy of the ionic subsystem. F_c is defined in Eq. (37). The total free energy (sum of the four previous contributions) is F, from which the experimental energy of the Be^{2+} ion at $T=0$ has been subtracted [$E(Be^{2+})=-27.311$ Ry]. Units are rydbergs.

T (eV)	Γ	Z^*	F_0	ΔF_i	F_c	F_{pair}	F
0.0	∞	2.000	+0.129	−29.330	0.048	−0.014	−1.856
2.5	18.81	2.000	−0.012	−29.360	0.031	0.263	−1.767
5.0	9.40	2.000	−0.403	−29.416	−0.010	0.409	−2.109
7.5	6.27	2.000	−0.993	−29.469	−0.069	0.546	−2.674
10.0	4.70	2.000	−1.737	−29.511	−0.139	0.686	−3.390
12.5	3.77	2.002	−2.605	−29.544	−0.218	0.831	−4.225
15	3.16	2.008	−3.580	−29.570	−0.306	0.979	−5.166
20	2.47	2.048	−5.841	−29.607	−0.509	1.308	−7.338
25	2.14	2.135	−8.553	−29.605	−0.748	1.691	−9.904
30	1.99	2.255	−11.757	−29.545	−1.023	2.135	−12.879
40	1.87	2.526	−19.613	−29.244	−1.686	3.183	−20.049
50	1.82	2.781	−29.179	−28.734	−2.485	4.401	−28.686
60	1.76	3.000	−40.178	−28.060	−3.404	5.748	−38.583
80	1.63	3.329	−65.479	−26.437	−5.527	8.703	−61.429
100	1.47	3.541	−93.877	−24.790	−7.916	11.849	−87.423

TABLE II. Free energy in Be at the density $\bar{\rho}=18.62$ g cm^{-3} ($c=9.58$), as a function of temperature. The electron-density parameter is $r_s=0.8529$ when $Z^*=2.088$. The various contributions are the same as in Table I. In the total energy F, the energy of the isolated Be^{2+} (-27.311 Ry) has also been subtracted. Units are rydbergs.

T (eV)	Γ	Z^*	F_0	ΔF_i	F_c	F_{pair}	F
0.0	∞	2.088	3.838	−29.878	−2.096	2.261	1.436
2.5	43.52	2.088	3.807	−29.895	−2.094	2.926	2.055
5.0	21.76	2.088	3.712	−29.913	−2.106	3.180	2.184
7.5	14.51	2.088	3.556	−29.935	−2.130	3.382	2.184
10.0	10.88	2.088	3.338	−29.967	−2.162	3.571	2.091
12.5	8.71	2.088	3.060	−30.004	−2.201	3.729	1.895
15.0	7.26	2.089	2.728	−30.047	−2.250	3.879	1.621
20.0	5.48	2.095	1.911	−30.157	−2.372	4.185	0.878
25.0	4.45	2.112	0.925	−30.318	−2.532	4.503	−0.111
30.0	3.82	2.142	−0.210	−30.540	−2.731	4.847	−1.323
40.0	3.12	2.235	−2.936	−31.174	−3.224	5.666	−4.357
50.0	2.76	2.352	−6.302	−31.982	−3.826	6.627	−8.172
60.0	2.55	2.475	−10.361	−32.874	−4.509	7.679	−12.754
80.0	2.28	2.705	−20.385	−34.679	−6.069	10.021	−23.801
100.0	2.10	2.901	−32.868	−36.317	−7.823	12.540	−37.157

These are displayed in the region of first neighbors. Even in this range of temperatures smaller than T_F, there is a significant change in the shape of the interaction, with an important damping of the Friedel oscillations as the temperature is raised.

The structural contribution F_{pair} in the fluid phase varies quite smoothly between 2.5 and 20 eV and it is tempting to extrapolate to $T=0$ in order to compare with the value calculated in the solid phase. But this is not possible for the following reason. Calculations for the one-component plasma (OCP) (Refs. 1–4) and the screened OCP (Refs. 5 and 6) show that F has an infinite derivative with respect to T at zero temperature. As a similar behavior may be expected in our model also, any extrapolation is hazardous. We conclude that the present results do not allow us to determine which phase is the most stable at low temperature. A complete determination of the phase diagram would require a more detailed study of the low-temperature domain, including the effect of the bridge function in the fluid phase, and a full treatment of vibrations in the solid phase. Such a study is outside the scope of the present paper devoted to plasmas.

In Table II, we give the various free-energy components at $c=9.58$. This compression corresponds to a free-electron density $\bar{n}=0.3848$ a.u. at $T=0$, that is exactly 10 times that of Table I. Here the electron gas is strongly degenerate ($T_F=68.9$ eV) in a large part of the domain of temperatures studied. The coupling constant Γ reaches a value of 43.5 at 2.5 eV and is still $\Gamma=2.10$ at

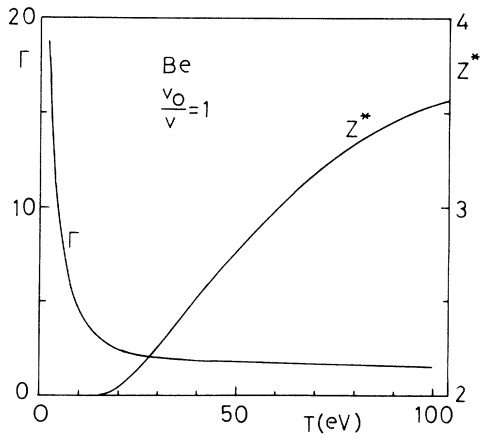

FIG. 14. Ionization of Z^* and ion-ion coupling constant Γ in Be, at normal density, as a function of temperature.

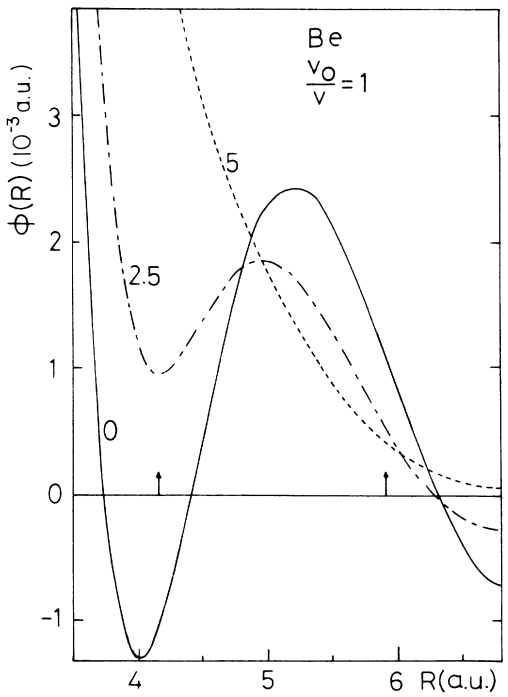

FIG. 15. Change in the pair interaction potential, for Be at normal density, when the temperature is raised form 0 to 5 eV. Solid curve, $T=0$; dot-dashed curve, $T=2.5$ eV; dotted curve, $T=5$ eV.

$T=100$ eV. At the highest density (Table II), the ionization Z^* is higher at low temperature (pressure ionization), but lower at high temperature than at normal density. The reason is that for a given $T>30$ eV, the $1s$ level population is larger because the Fermi energy is significantly higher and the $1s$ eigenvalue not very different. Table II shows a free energy F at low temperature ($2.5\leq T\leq 7.5$ eV), which increases with T. Fortunately, this does not imply that the entropy of the fluid is negative, because F does not contain the ideal contribution. With that contribution included, F becomes monotonic.

The only calculation including the structural F_{pair} with which we can try to compare our results for Be is the Monte Carlo calculation of Hubbard and DeWitt.[5] These authors treated the case of a mixture of hydrogen and helium ions interacting via Coulomb potentials linearly screened with the RPA dielectric constant at zero temperature. They give a fit of their results for the internal energy and Helmholtz free energy. We can use this fit, applied to the case of pure He, to mimic our Be results when Z^* is not too different from 2. (Their fit contains explicitly the ion charge Z^*.) But we must add a correction to their results, before comparison, for taking into account the effect of core electrons in Be. To estimate that correction, we assume that the electron-ion interaction in Be can be modeled by an Ashcroft empty core model potential with a core radius $R_c=0.5$ a.u. To first order in the pseudopotential, the correction to the excess free energy is

$$\delta F_{\text{exc}}=\bar{n}\int_0^{R_c}\frac{Z^*}{r}4\pi r^2 dr\ ,$$

which gives $\delta F_{\text{exc}}=0.24$ Ry at $\bar{\rho}_0$ ($Z^*=2$) and 2.52 Ry at $10\bar{\rho}_0$ ($Z^*=2.088$). We must also say that the numerical fit of Hubbard and DeWitt is based on Monte Carlo runs covering a given domain of densities and temperatures, and that we used the fit in part outside that domain. In our calculation, the excess free energy to consider is

$$\delta F_{\text{exc}}=\Delta F_i+F_c+F_{\text{pair}}-E(\text{Be}^{2+})\ ,$$

where the energy of the Be^{2+} free ion is subtracted. Results are shown in Table III for temperatures where the comparison is possible, that is, temperatures much smaller than the Fermi temperature. Substantial differences are apparent. We think that the main causes are (i) the difference in electron screening (linear in Ref. 5, nonlinear in the present work), which gives quite different displaced electron densities around the ions,[37] and (ii) core othogonalization effects: we have made a crude first-order correction to the results of Ref. 5, but these effects are still not included in the pair interaction, which is likely very different from ours. More meaningful comparisons would be very useful. Similar calculations for Al plasmas are currently in progress and will be reported in a subsequent publication, together with more information on other important thermodynamic functions, such as internal energy and pressure.

V. CONCLUSIONS

We tried to show that the NPA picture of liquid simple metals may be extended for describing plasmas in ranges of densities and temperatures where their electronic structure remains "simple." The main new features of the model when applied to plasmas are (i) the temperature-dependent self-consistent calculation of the electron charge density (for liquid metals, the electron density at zero temperature is in general used), (ii) the determination of a density and temperature-dependent ionization state Z^*, (iii) the calculation of the pair interaction for every $\bar{\rho}$-T plasma state, and (iv) the computation of the ionic part of the Helmholtz free-energy using the HNC equation (in liquid metals, use is often made of a reference system).

When applied to the solid phase at zero temperature, the model reproduced quite well the total energy curve $E(\bar{\rho})$ for Be and Al, in the range of densities where it might be expected to work. This supports the reliability of the prescription made for calculating $Z^*(\bar{\rho},T)$. Results for the pair interaction potentials $\phi(r)$, and for the various contributions to the Helmholtz free energy, are presented for a number of $\bar{\rho}$-T conditions in the Be plasma.

Future work has to be done in the following directions. First, it will be useful to test the influence of corrections to the HNC equation (Bridge terms). For the cases presented here, we think they will not be too large because the screening of the interaction is strong so that,

TABLE III. Comparison between excess free-energy results of the present work and those of screened OCP theory for helium, applied to the case of Be with a pseudopotential correction in first order. Our value of Z^* is used in the formula of Ref. 5 for the excess free energy derived from the screened OCP Monte Carlo simulation. Units are rydbergs.

	$\bar{\rho}=\bar{\rho}_0$			$\bar{\rho}=9.58\bar{\rho}_0$	
T/T_F	Present work	Screened OCP	T/T_F	Present work	Screened OCP
0.169	−1.755	−3.372	0.036	−1.752	−4.945
0.337	−1.706	−3.185	0.072	−1.528	−4.715
			0.109	−1.372	−4.513
			0.144	−1.247	−4.316
			0.182	−1.165	−4.116
			0.218	−0.468	−3.915

even for the highest Γ values which have been met, the "effective" coupling is much smaller than for an OCP with the same Γ. Second, we would like to compare our results with those obtained by others who use linear screening theories. But we think that this comparison may be relevant only if linear theory is applied to pseudopotentials (or model potentials) for metals, and not to bare electron-ion Coulomb interactions. Finally, a lot of work remains to be done to provide comprehensive results for the equation of state of these plasmas. The internal energy and pressure have to be computed. Each of these thermodynamic functions includes a part which can be calculated directly because the free energy ΔF_i has stationary properties with respect to Δn and the Kohn-Sham eigenstates. But another part has to be calculated by taking explicit derivatives with respect to T or $\bar{\rho}$ (for instance, the part coming from the T-$\bar{\rho}$ dependence of Z^*). Further studies along these lines, which will require very substantial computations, are currently in progress.

ACKNOWLEDGMENTS

The author is very indebted to Professor Callaway, Professor H. DeWitt, Professor N. March, and Dr. M.W.C. Dharma-wardana for a careful reading of the manuscript and many useful comments. This research was supported in part by the National Science Foundation under Grant No. PHY82-17852, supplemented by funds from the National Aeronautics and Space Administration, at the University of California at Santa Barbara.

[1]S. G. Brush, H. L. Salin, and E. Teller, J. Chem. Phys. **45**, 2101 (1966).
[2]W. L. Slattery, G. D. Doolen, and H. E. DeWitt, Phys. Rev. A **21**, 2087 (1980).
[3]J. P. Hansen, Phys. Rev. A **8**, 3096 (1973).
[4]J. P. Hansen and I. R. McDonald, Phys. Rev. A **23**, 2041 (1981).
[5]W. B. Hubbard and H. E. DeWitt, Astrophys. J. **290**, 388 (1985).
[6]H. E. DeWitt and F. Rogers, Phys. Lett. A **132**, 273 (1988).
[7]H. Iyetomi and S. Ichimaru, Phys. Rev. A **34**, 433 (1986).
[8]M. W. C. Dharma-wardana, F. Perrot, and G. C. Aers, Phys. Rev. A **28**, 344 (1983).
[9]J. Chihara, Phys. Rev. A **33**, 2575 (1986), and references therein.
[10]N. W. Ashcroft and D. Stroud, Solid State Phys. **33**, 1 (1978), and references therein.
[11]M. Rasolt and R. Taylor, Phys. Rev. B **11**, 2717 (1975).
[12]L. Dagens, M. Rasolt, and R. Taylor, Phys. Rev. B **11**, 2726 (1975).
[13]J. Moriarty, Phys. Rev. B **16**, 2537 (1977).
[14]M. Manninen, P. Jena, R. P. Nieminen, and J. K. Lee, Phys. Rev. B **18**, 7057 (1981).
[15]L. Dagens, J. Phys. F **6**, 1801 (1976); **7**, 1167 (1977).
[16]J. Moriarty, Phys. Rev. B **38**, 3199 (1988).
[17]R. M. More, Adv. At. Mol. Phys. **21**, 305 (1985); R. M. More, in *Atomic and Molecular Physics of Controlled Nuclear Fusion*, edited by C. J. Joachain and E. Post (Plenum, New York, 1983) p. 399.
[18]L. Dagens, J. Phys. (Paris) **34**, 879 (1973).
[19]W. Kohn and L. J. Sham, Phys. Rev. A **140**, 1133 (1965).
[20]N. D. Mermin, Phys. Rev. A **137**, 1441 (1965).
[21]J. M. Ziman, Proc. R. Soc. London **91**, 701 (1967).
[22]L. Dagens, J. Phys. C **5**, 2333 (1972).
[23]L. Dagens, J. Phys. (Paris) **36**, 521 (1975).
[24]W. A. Harrison, *Pseudopotentials in the Theory of Metals* (Benjamin, New York, 1966).
[25]M. Manninen, Phys. Rev. B **34**, 8486 (1986).
[26]K. W. Jacobsen, J. K. Norskov, and N. J. Puska, Phys. Rev. B **35**, 7423 (1987).
[27]J. D. Kress and A. E. DePristo, J. Chem. Phys. **88**, 2596 (1988).
[28]W. Jones and N. H. March, Proc. R. Soc. London Ser. A **317**, 395 (1970).
[29]V. Heine and J. E. Shiveley, J. Phys. C **4**, 1263 (1972).
[30]R. Balian and C. De Dominicis, Ann. Phys. (N.Y.) **62**, 229 (1971).
[31]F. Perrot, Phys. Rev. B **16**, 4335 (1977).
[32]F. Perrot and M. Rasolt, Phys. Rev. B **23**, 6534 (1981).
[33]F. Perrot, Phys. Rev. B **21**, 3167 (1980).
[34]J. Meyer-ter-Vehn and W. Zittel, Phys. Rev. B **37**, 8674 (1988).
[35]A. K. McMahan and M. Ross, in *High Pressure Science and Technology*, edited by K. Timmerhaus and M. S. Barber (Plenum, New York, 1979), Vol. 2.
[36]W. Kohn and C. Majumdar, Phys. Rev. **138**, A1617 (1965).
[37]F. Perrot, Phys. Rev. A **25**, 489 (1982).
[38]M. W. C. Dharma-wardana and F. Perrot, Phys. Rev. A **26**, 2096 (1982).
[39]S. Ichmaru, Rev. Mod. Phys. **54**, 1017 (1982).
[40]S. Tanaka and S. Ichimaru, J. Phys. Soc. Jpn. **53**, 2039 (1984).
[41]T. Morita and K. Hiroike, Prog. Theor. Phys. **23**, 1003 (1960).